

Conductive and Porous SnCu-Coated Carbon Cloth Network for Binder-free Li-Ion Storage Anodes

Venroy Watson¹, Wete Telama¹, Yaw Yeboah¹, Jim Zheng², Egwu Eric Kalu^{1,*}

¹ Department of Chemical and Biomedical Engineering, FAMU-FSU College of Engineering, 2525 Pottsdamer St., Tallahassee, FL 32310

² Department of Electrical and Computer Engineering, FAMU-FSU College of Engineering, 2525 Pottsdamer St., Tallahassee, FL 32310

*E-mail: ekalu@eng.famu.fsu.edu

Received: 25 July 2018 / Accepted: 16 November 2018 / Published: 5 January 2019

Large volume change occurs during lithiation/delithiation of Sn anodes and result in pulverization, poor cycling, capacity loss and anode degradation that impedes the general use of Li-ion batteries. This study proposes a time-controlled synthesis approach for 1-D SnCu nanoparticles on three-dimensional anode by electrolessly adhering Cu to C cloth and subsequently Sn on the Cu. After annealing at 200 °C, electrically conductive, porous, flexible and mechanically stable CuSn alloy anode results. The CuSn anodes exhibited high conductivity due to copper deposit, accommodated volume changes and stress due to both 1-D-deposit and porosity and have high electrochemical activity due to large surface area. After 100 cycles, the sample deposited for the shortest time (1.5 min) interval and close to 1-D SnCu deposit has a specific discharge capacity of ~605 mAh g⁻¹ which contrasts to the ~400 mAh g⁻¹ obtained for the sample deposited for 6 min. The specific electrode surface area of the 1.5 min sample was 169 m² g⁻¹ in contrast to 6.4 m² g⁻¹ obtained for the 6 min sample. A rate capability of 520 mAh g⁻¹ at a current density of 583 mA g⁻¹ was achieved for the thinnest deposit. The porous Sn anode materials demonstrated low resistance during electrochemical impedance analysis and showed high reversible redox reactions during cyclic voltammetry tests. The achievement of high capacity anode (comprising of Sn-SnO₂-Cu₆Sn₅) with good reversible capacity retention through electroless coating method indicates that electroless deposition on flexible free-standing and porous substrate is an effective Sn anode fabrication technique.

Keywords: Sn anode; Electroless deposition; Cu-Sn alloy; cyclability; binder-free

1. INTRODUCTION

Lithium ion batteries (LIBs) are presently considered as one of the most viable choices of energy storage devices for applications ranging from electronics, grid storage and motor vehicles. High power, high energy densities, and lightweight are some of the characteristics that make LIBs suitable for electric

vehicle (EV) applications [1-4]. The advancement in the development of LIBs is hindered by several factors including but not limited to the performance of the electrodes. Currently, the LIB cathode chemistries are very well established and research investigations on cathodes are generally and vigorously geared towards improving the cathode performances [1,5-8].

However, in addition to the cathode, the performance of the battery including its capacity is also dictated by the nature and chemistry of the anode materials [9]. For instance, during a reversible reaction in the lithium ion battery, the anode receives and releases lithium ions via the following reaction:



where M can be any of the several materials that can form an alloy with Li including C, Si, Ge, Mg, Pb, Al, Sn, Sb, Pt, Ag, In, or Zn [9-21]. The most common anodic material of choice is graphitic or carbonaceous materials chosen for its low cost, flat and low working potential and long cycle life [13]. But graphite for example, offers only a capacity of 372 mAh/g which is a limitation where a high capacity and power density may be required. Thus, the use of a low capacity anode material lowers the performance of LIBs. Although other anode materials exist as stated earlier, they are not however as cheap as carbon materials nor can they provide low and flat potential as carbon. Furthermore, some of these graphite alternatives are costly to fabricate and may not be environmentally benign [14-16]. One very attractive anode material is Tin (Sn) [13]. Sn offers much higher capacity (991 mAh/g) than graphite during lithiation. This higher capacity per gram makes Sn an ideal candidate for use in lithium ion batteries, especially in lightweight applications. Furthermore, Sn anodes may also be used in other battery chemistries including sodium battery, for example.

Despite Sn's positive attributes, its anodes suffer from large volume expansion of up to 350% and loss of electrical contact during lithiation and delithiation. The large volume expansion can lead to the pulverization of the anode surface thereby resulting in low coulombic efficiency and drastic loss of capacity. Furthermore, volume expansion lowers the cycling stability of Sn anodes [1, 9]. Efforts to address and improve Sn anode performance have been geared towards: 1) the use of nanometer size Sn or SnO₂ particles in electrode composites offering higher surface area and stress accommodation [1,9]; 2) the inclusion of an electrically transporting and Li⁺ inactive/active phase or matrix with capabilities to buffer Sn's expansion [1]; and 3) the use of porous three-dimensional templates allowing the tailoring of Sn-based electrode material synthesis techniques meanwhile providing a material with deep penetration pathways for electrolytes and short Li⁺ transport [1]. For example, silicon-SnO₂ coated nanotubes, carbon fibers or carbon tubes filled with SnO₂ or Sn, and Sn in carbon nanospheres have been investigated as Li-ion battery anode material [9,22-24] for the case of tailoring the synthesis method to obtain nanoparticles. For templated synthesis, recently, Chen et al. used electrodeposition method to deposit Sn on Tobacco Mosaic Virus (TMV) with a nickel current collector. This resulted in improved cyclability of the Sn anode with limited capacity performance [10]. In addition, Shin et al [25] and Xue et al [26] used electrochemical method to deposit Sn on 3D Cu foam and 3D Cu sponge (templates that offer opportunities to engineer Sn-based electrodes), respectively. The resulting Cu-Sn alloy materials were used as anodes in lithium ion batteries. However, long-term cyclability or capacity retention was limited [25,26] as exhibited by the Sn-based templated anodes. Further, they did not examine how the single-phase Cu-Sn intermetallics and thickness of Sn deposit affect the capacity and long-term cyclability of the Sn anodes.

Other Sn compounds and intermetallic Sn alloys have been pursued to mitigate tin's pulverization [17-21] in anode materials. Literature studies on tin anode materials such as SnSb and composites materials of SnSb:M, (where M = Ni, Co, Fe, Si, CNT) have demonstrated promising performances [18,19]. Recently, Nithyadharseni et al. [18] used a reductive co-precipitation approach in the presence of metal chlorides and sodium borohydride reducing agent to fabricate nano-size intermetallic alloys containing SnSb:Fe, SnSb:Co, and SnSb:Ni. Interestingly, it was found that the first discharge capacity (lithium insertion) for intermetallic alloys with SnSb:Fe, SnSb:Co, and SnSb:Ni were ~1680, ~2630 and ~1565mAh/g, respectively. Similar to Cu-Sn alloys, the SnSb and SnSb:M anode materials have also demonstrated some limitations in their performances.

As a result of these shortcomings with Sn anodes, it can be deduced that several performance issues (such as reversible long-term cycling with less pulverization, optimal ratio of 2nd phase buffer to Sn, maintenance of electrical contact during repeated cycling and having nanosized high surface area strain reducing films or particles), have not been addressed. These are fundamental fabrication and cost related issues that are vital to the success of Sn anodes. Furthermore, limited investigations have been carried out on other compatible substrates or scaffold for engineering of suitable Sn anode materials. A concept yet to be fully explored is the control of the single-phase Cu-Sn intermetallic films or particles and the adjoining Sn thickness during the deposition of very small amount of Sn nanoparticles on a flexible (including 3-D) porous substrate. The porous substrate and the deposited nanosized Sn particles are capable and favored to allow the Sn deposit to expand and contract without allowing those events that lead to Sn pulverization to occur. As a result, we intend to tailor electrode fabrication technique to better understand how to avoid excess Sn deposit (i.e. Sn deposit above that required for predominant existence of single-phase Cu-Sn intermetallics) that can severely impede the electrochemical performance of Li battery anode. The deposited Sn influence key parameters such as mass loading, electrical conductivity, particle size and surface areas, optimal ratio of the buffer phase (e.g Cu) to Sn for best performance and transport of lithium ions needed for electrode performance. In our most recent investigation [1], we demonstrated the feasibility of electroless deposition of Sn on copper-coated graphite particles as a potential anode material for LIBs. In the report, the expansion of Sn in the anode (Sn-Cu@graphite) composite was buffered by copper leading to more than 300 reversible cycles at high coulombic efficiencies.

As commonly known, several approaches including ball milling, thermal treatment of copper and tin particles, electrodeposition, sputtering, or solution (chemical) reduction are some of the commonly used methods for the synthesis of copper-tin anode materials [1, 2, 27]. However, in this study, we explore the fabrication of Sn anodes via electroless coating of Sn on copper-coated woven carbon cloth and its subsequent material and electrochemical characterizations. Even though previous researchers have used the very promising electrodeposition approach to coat Sn on Cu foam or mesh, key concepts delineated above that are needed to influence electrode performance by tailoring the synthesis to achieve the best Sn-based anodes using a templated approach has not been fully explored. Carbon cloth has an established electronic network and is a stable freestanding substrate with voids. With a light coating of Sn on the Cu coated carbon substrate, these voids can be left standing without compromising on the current carrying ability of the carbon substrate. Also, carbon cloth is cheaper and lighter than porous or 3D copper scaffold that has been commonly used as substrate for Sn deposition. Unlike the previously

reported classical anode fabrication methods requiring a binder to hold the composites together, the electroless coating method on woven or non-woven carbon cloth does not need binders. The electroless method bypasses the use of the wet chemistry method (mixing a slurry) or the conventional doctor blade method that utilizes carcinogenic N-methyl pyrrolidine (NMP) to dissolve the polyvinylidene fluoride (PVDF) that binds the electrode composite or other solvents used for polytetrafluoroethylene (PTFE) dissolution. Furthermore, electroless method does not consume as much energy to drive the deposition process. Instead, we take advantage of the natural thermodynamics of the electrochemical reactivity series where, Sn chemically displaces Cu by using an acid solution and thiourea to reverse the Sn and Cu deposition potentials [27,28]. This process that can be carefully controlled on the amount of Sn deposited results in complete coating of Cu surface with Sn. Our results show that by varying the Sn deposit (equivalent to varying deposition time of Sn - 1.5 min, 3 min, 6 min), anodes made using Sn-Cu coated carbon cloth outperformed uncoated carbon cloths. The key performance parameters that play a role in the electrode performances that result from the modification of the carbon substrate with electroless Cu-Sn deposit include copper-tin ratio and mass loading, electrode electrical conductivity and surface area, deposited particle sizes, Sn tube diameter, curvature, and Li⁺ mobility. It is to be noted that our approach that uses deposited nanoparticle size Sn on Cu differs from other methods in which nanometer size Sn or SnO₂ particles in electrode composites are used to offer higher surface area and stress accommodation [9].

2. EXPERIMENTAL SECTION

2.1 Raw materials

Ready to use AvCarb 1071 HCB carbon cloth was purchased from Fuel Cell Earth LLC (MA, USA). Palladium acetate, ammonium hydroxide, copper sulfate pentahydrate, ethylenediaminetetraacetic acid (EDTA), 2,2-bipyridyl, sodium hypophosphite, thiourea, and stannous sulfate were purchased from Sigma Aldrich Corporation. Dimethylformamide (DMF), 99.5% methanol (CH₃OH), and 90% nitric acid were also purchased from Sigma Aldrich Corporation. 1.0 molar lithium hexafluorophosphate (LiPF₆) dissolved in ethyl carbonate and dimethyl carbonate was obtained from BASF Corporation. In addition, glass fiber separator was purchased from EL-CELL Corporation. All materials utilized in this experiment were of research rating and did not require further refinement.

2.2 Sn anode preparation

Cu was electrolessly deposited on to an activated carbon cloth. The carbon cloth was activated using an ink with the following composition: 50 g poly-vinyl butyral, 250 mL methanol, 5 mL sodium hydroxide, and 0.5 g palladium acetate. The activated cloth was put in an oven at 350 °C for 24 hours to generate Pd nanoparticles required for initial nucleation of electroless copper. The substrate was subsequently immersed in an electroless copper plating bath for 1 hour at 25 °C. The composition of the electroless copper bath had 5.99 g/L of copper sulfate pentahydrate, 26.99 g/L of EDTA, 48.9 g/L of

formaldehyde, and 0.05 g/L of 2,2-dipiridyl nitric acid solution. After deposition, the Cu plated cloth was rinsed in deionized water and dried at 71°C for 24 hours.

To prepare the Sn coated Cu material, the Cu coated cloth was immersed in a tin bath composed of 28 g/L of stannous sulfate, 80 g/L of sodium hypophosphite, and 80 g/L of thiourea. Prior to being coated with Sn, the Cu coated cloth was cut in discs of 1.27 cm². To control the amount or thickness of Sn deposit on the copper plated substrate, the immersion times of the discs in the Sn bath were varied or controlled. In the present work, three discs were immersed in the tin bath at 25 °C for 1.5 minutes, 3 minutes, and 6 minutes, respectively. The Cu-Sn cloth was dried at 71°C for 24 hours. This was followed by annealing at 200 °C for 2 hours. From here on, copper cloths coated with Sn will be designated as Sn 1.5 min, Sn 3 min, and Sn 6 min signifying the Sn deposition times of 1.5 minutes, 3 minutes, and 6 minutes, respectively. To determine the quantity of Cu and Sn deposited, disc samples were weighed before and after Cu and Sn depositions. It was found that the combined mass of Cu and Sn deposited on the 1.27 cm² discs electrodes were 4.6 mg, 5.14 mg and 6.3 mg, respectively for the Sn 1.5 min, Sn 3 min, and Sn 6 min anodes. In addition, these weights correspond to 24%, 26% and 30.1% of the anodes' weight for the Sn 1.5 min, Sn 3 min and Sn 6 min, respectively.

2.3 Material characterizations

On the completion of electrode fabrication, morphological characterization was conducted wherein the electrodes were photographed and physically assessed. Morphology of the electrodes' surfaces was obtained using a ZEISS 1540 scanning electron microscopy (SEM). Furthermore, energy dispersive spectroscopy (EDS) was performed to determine the elemental composition/presence of the deposited metals. The phase or structural characterization of the deposits was determined using X-ray diffraction (XRD) and the patterns were captured via Siemens model D500 θ-2θ goniometer. Specific surface areas of the carbon cloth (barecloth) and Sn-Cu coated carbon cloth were obtained using the nitrogen adsorption/desorption isotherms performed in Autosorb iQ² Quantachrome Instrument.

2.4 Electrochemical characterizations

Four-point probe consisting of a Keithley 2700 multimeter data acquisition system connected to a Newport 460A probe was used to measure resistance. Resistance was used to calculate sheet resistivity and conductivity of the barecloth, Cu coated cloth, and Sn coated electrodes. Coin cells (type CR 2032) were fabricated and used to study the electrochemical performances of all fabricated electrodes. The coin cell assembly consisted of Cu-Sn coated cloth disc of area 1.27 cm² laminated to Cu current collector and dried under vacuum. Coin cells were assembled in an argon filled glovebox using Cu-Sn coated cloth as cathode, Li metal as anode (two electrodes setup) and membrane separator (glass fiber) with 18 mm (diameter) × 1.55 mm (thickness). Electrolyte made of 1 molar lithium hexafluorophosphate (LiF₆P) in dimethyl carbonate (DMC) and ethyl carbonate (EC) was used.

Using a potential ranging from 0.007 V-1.20 V (vs Li/Li⁺), electrochemical performance of the coin cells was measured throughout charging and discharging with Neware battery testing analyzer

(linked to a Compaq computer) with 5 V and 10 mA as the respective, unit's maximum voltage and current. Cyclic voltammetry (CV) and electrochemical impedance spectroscopy (EIS) analyses were obtained using Gamry Instruments Reference 3000 Potentiostat/Galvanostat/ZRA. CV analysis was completed at 0.5 mVs⁻¹ within 0 V and 1.5 V. Additionally, at 100% state of charge EIS was performed from 10⁶ Hz to 0.01 Hz. All characterizations were achieved at room temperature.

3. RESULTS AND DISCUSSIONS

3.1 Cu and Sn electroless deposition pathway forming Sn-Cu coated C cloth anode material

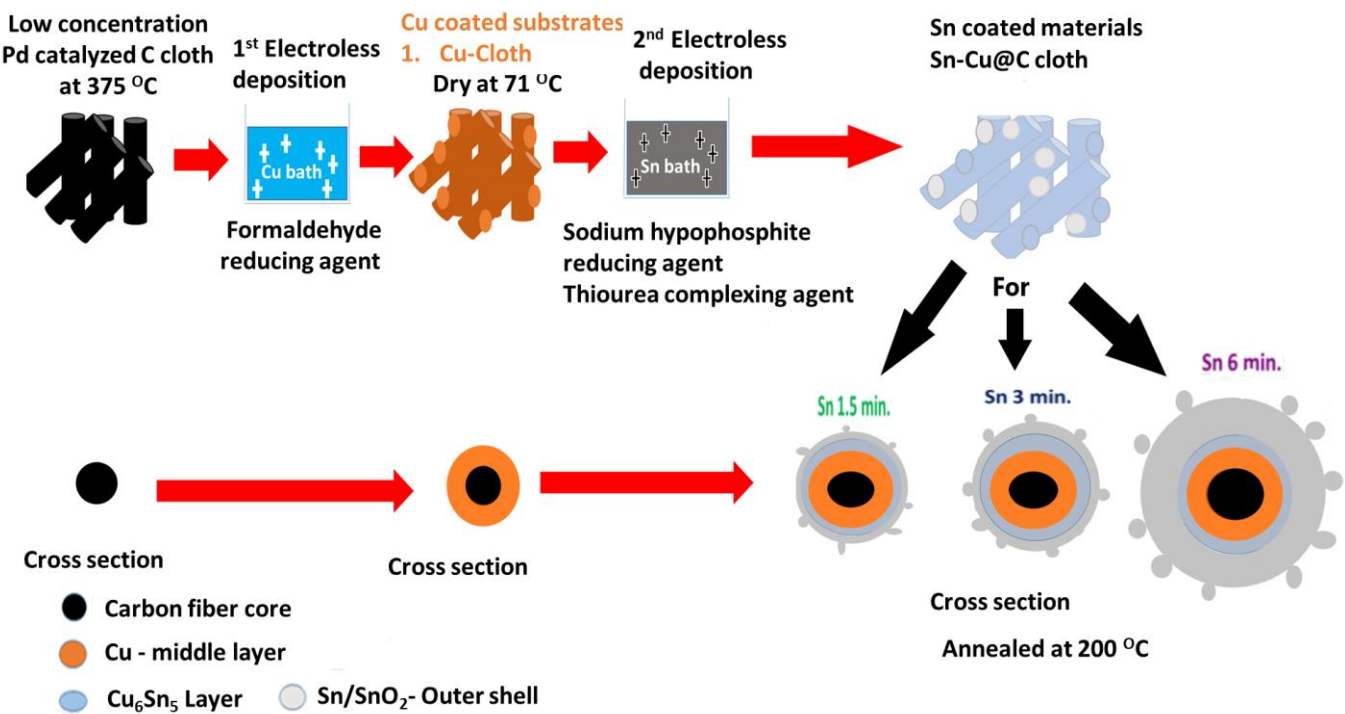
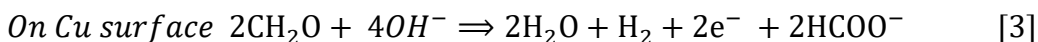
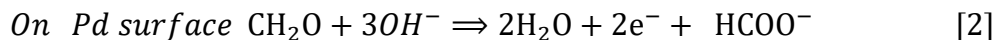


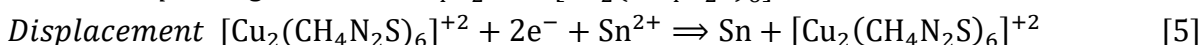
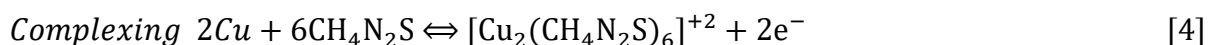
Figure 1. Animation schematizing the electroless deposition and the heat treatment of electroless Cu and Sn deposits resulting in the formation of anode material made of Sn, SnO₂ and Sn-Cu alloys coated C cloth.

As mentioned previously, several approaches including ball milling, thermal treatment of copper and tin particles, electrodeposition, sputtering, or solution (chemical) reduction are some of the commonly used methods for the synthesis of copper-tin anode materials [1, 2, 27]. In this investigation, we have implemented the electroless (chemical reduction) coating procedure to obtain intermetallic of Cu₆Sn₅, Sn, and SnO_x, (where x can be 1 or 2) [1, 27, 28]. The electroless coating offers simplistic, inexpensive, and environmentally friendly process for the fabrication of Sn anode materials. To begin, a low amount of Pd (< 40 µg/cm²) was used to make the mesh-like carbon cloth active for electroless deposition. As soon as Pd catalyzed C-cloth was placed in the copper sulfate bath containing formaldehyde, formaldehyde was immediately oxidized on the surface of Pd seeding catalyst thus releasing 2e⁻. In a reduction reaction process, these 2e⁻ are taken by the Cu ions in the solution and this

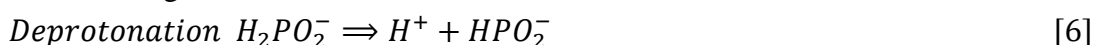
resulted in coating of Cu on the Pd catalyzed C-cloth's surface. This is depicted in Fig.1 for the first electroless (Cu) deposition step [29], The formaldehyde reducing agent can be autocatalytically oxidized by the already deposited Cu, thereby reducing Cu ions while increasing Cu plating on the surface of the porous mesh-like C cloth. Eqs. 2 and 3 govern the oxidation of formaldehyde and the deposition of Cu on Pd and Cu surfaces [1,29].



Electroless Cu deposition on C cloth was followed by the electroless deposition of Sn on the Cu-coated C cloth (Fig. 1). The electroless deposition of Sn on Cu utilizing sodium hypophosphite (reducing agent) and thiourea (complexing agent) occurs in two reaction stages according to Zhao et al [27]. At first, a displacement reaction transpires and secondly, a reduction reaction occurs [27]. During the displacement reaction, copper complexes with thiourea and consequently, Cu ions are released in the solution. The complex of copper thiourea works to dislocate ions of Sn, meanwhile, Sn ions deposited on the Cu-coated C cloth surface forms a layer of CuSn alloy at the interface of Cu and Sn which can be of micrometer thickness. Eqs. 4 and 5, capture the complexing and displacement reactions, respectively. As generally recognized, thiourea as an active complexing agent is instrumental in this process, because it drops the standard electrochemical potential of Cu^+/Cu below that of Sn^{2+}/Sn hence the displacement reaction is facilitated [1,27].



The second phase of the electroless deposition ensues when ions of Sn undergo reduction by sodium hypophosphite ion, and simultaneously the hypophosphite ion undergoes oxidation. In this process hypophosphite ion deprotonates yielding hydrogen free radicals as shown in Eqs. 6, that are responsible for the reduction of Sn ions [1,27]. The formation of Cu_6Sn_5 intermetallics and pure Sn/SnO_x coating on Cu C cloth as shown in Fig. 1 is achieved through the combined displacement and reduction reactions during the electroless deposition of Sn and finally heat treatment at 200 °C. While the Cu_6Sn_5 intermetallics exist only at the interface between Cu and Sn deposits, the rest of the deposit is made up of the Sn/SnO_2 coating [1].



3.2 Morphological and structural characterizations

The image in Fig. 2a shows that uniformly Tin-coated carbon cloth was synthesized. This was achieved by starting with bare carbon cloth (barecloth) followed by electroless copper deposition on the cloth and finally a preferential displacement of Cu by Sn electrolessly while the Cu is exposed to the solution of Sn in the bath. The carbon cloth (black) observed in the image changed color to reddish-brown indicating the deposition of Cu and then to shiny/light gray after Sn deposition. Fig. 2b presents the mechanical stability and flexibility of the barecloth, Cu cloth, and Sn coated Cu cloth disc electrodes. All electrodes were easily bent in halves and they regained their original shape very easily without breaking or fracture.

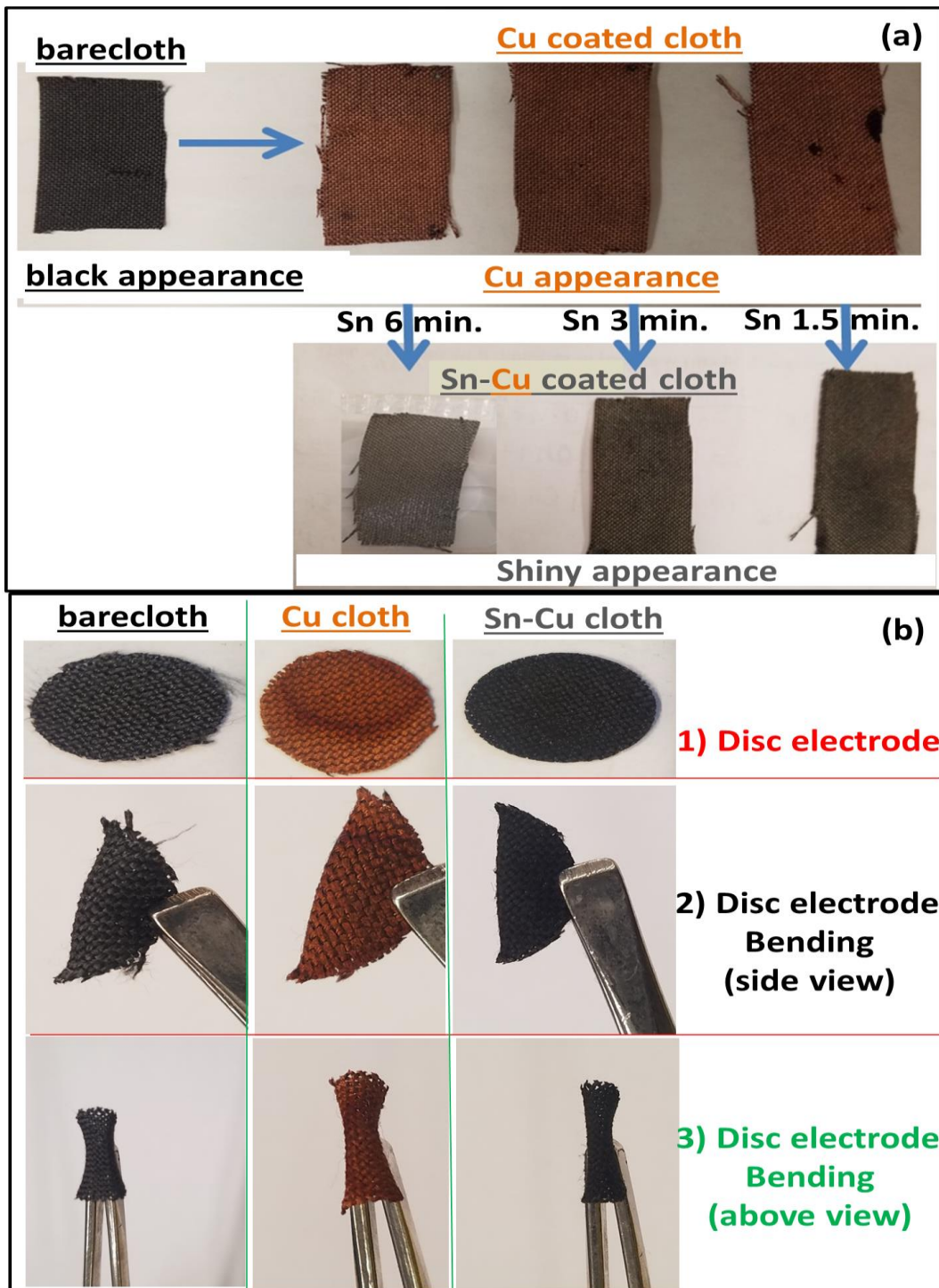


Figure 2. (a) Images of synthesized flexible, free standing and thin Sn anode showing barecloth, Cu coated cloth and freshly Sn-coated cloth (1.5 min, 3 min, 6 min), (b) bending of barecloth, Cu cloth, and Sn-coated Cu cloth disc electrodes.

SEM was performed to determine the morphological characteristics of the barecloth and the electrolessly coated cloths as shown in Fig. 3. The identity of each individual sample is indicated on the top left corner of the image in Fig. 3. The diameter of the barecloth fibers was approximately 6.5 μm and after Cu deposition the cloth fiber diameter increased to approximately 7.5 μm . Following the

deposition of Sn on the Cu-coated cloth, the fiber diameters ranged from 8 μm to 10 μm for the 1.5 min–6 min deposition times. Increase in fiber diameters indicates the successful deposition of both Cu and Sn electrolessly. After 1 hour, the copper deposit uniformly covered the carbon fibers (Fig. 3b). For the Sn coated cloths we see an increase in the particle size of Sn deposited. It appears that both the coating thickness and particle size grew with increasing deposition time. The average particle sizes for Sn 1.5 min, Sn 3 min, and Sn 6 min samples determined from SEM were approximately 75 nm, 128 nm and 270 nm, respectively. It is evident that changes occur in the surface texture of the substrate going from barecloth (smooth surface) to Cu cloth (with even and slight rough Cu coating) then to Sn-Cu coated cloths (more bumpy/rough and shiny particles with increase in deposition time).

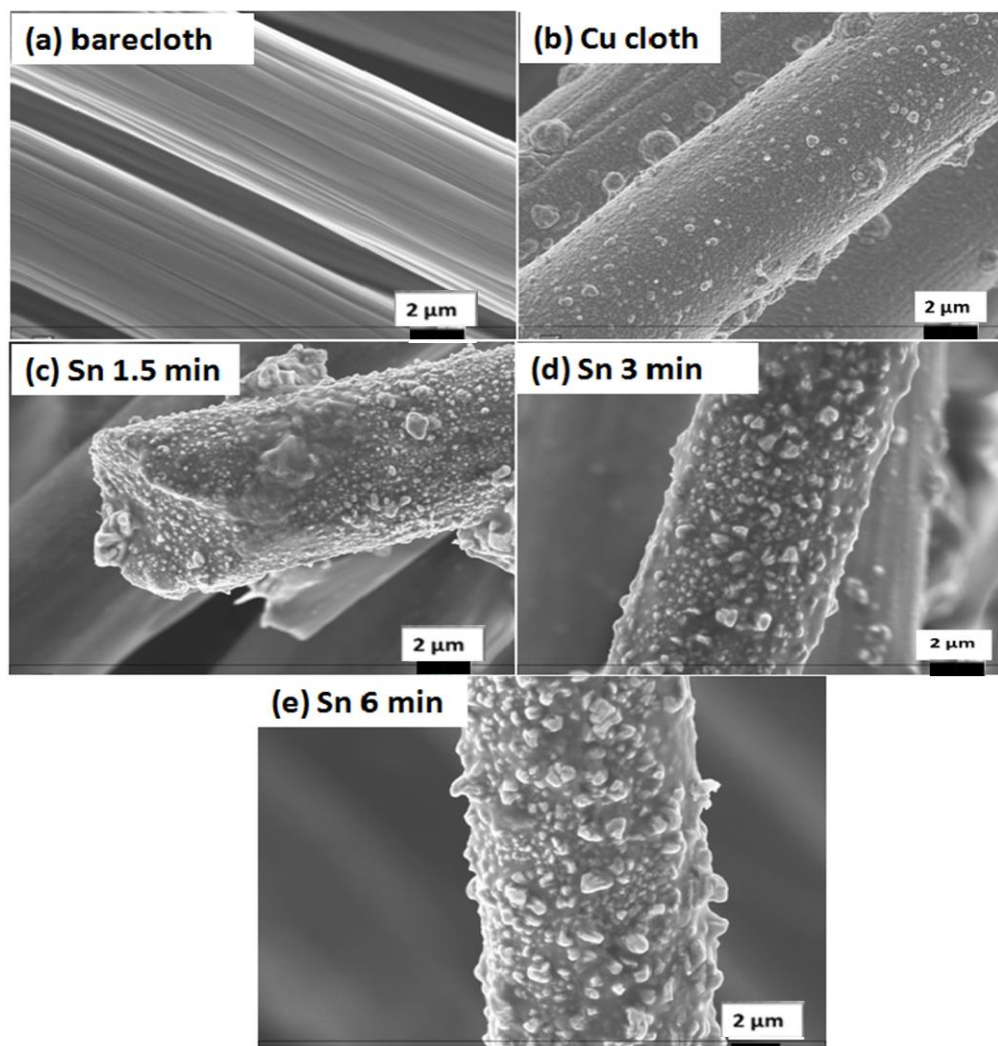


Figure 3. SEM showing the morphology of (a) barecloth, (b) Cu coated cloth (c) Sn 1.5 min, (d) Sn 3 min, and (e) Sn 6 min.

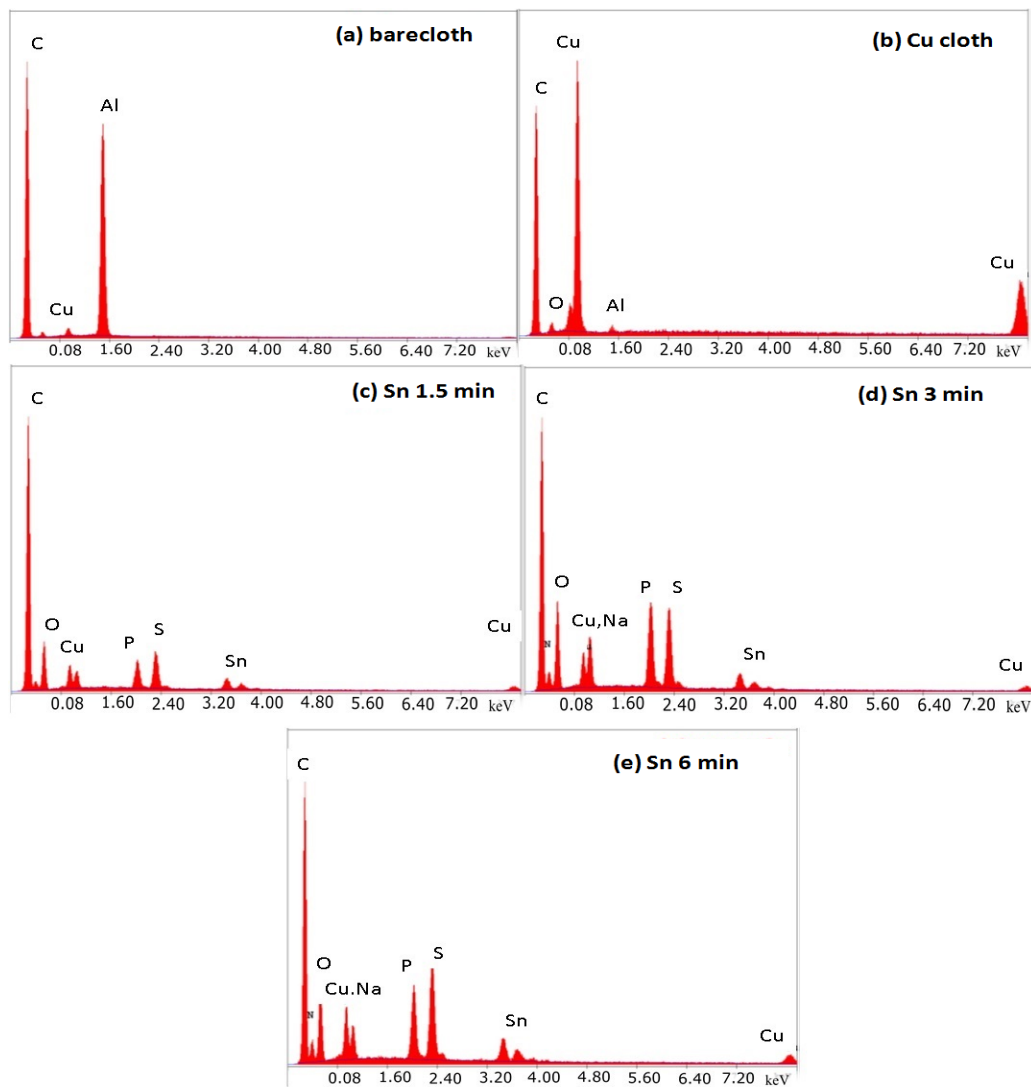


Figure 4. EDS spectra corresponding to (a) barecloth, (b) Cu coated cloth (c) Sn 1.5 min, (d) Sn 3 min, and (e) Sn 6 min.

The EDS spectra for the barecloth and electrolessly coated cloths are shown in Fig. 4. As expected, a C peak dominates Fig. 4a since the barecloth is made of carbon. The negligible Al and Cu peaks are due to the Al stage and Cu paste used to hold the sample. For Cu cloth, the dominating Cu peak in Fig. 4b is expected since copper was electrolessly deposited as supported by the photograph in Fig. 2. All the Sn-coated samples exhibit an increase in Sn and O₂ peaks as shown in Fig. 4c-e. EDS results indicate Sn constitute 9.02 wt. %, 15.75 wt. %, and 28.45 wt. % for the Sn 1.5 min, Sn 3 min and Sn 6 min anodes, respectively. These results correspond very well with the experimentally measured wt. % composition obtained after electroless Sn deposition. This confirms that the amount of Sn deposited on carbon cloth increases with increase in deposition time. Peaks related to Na, N, S, and P are present and are believed to be residual amounts from the electroless tin and copper baths as their EDS wt. % were well below 1%.

XRD analysis was performed to determine the structure of the coated and uncoated carbon cloth as shown in Fig. 5. Fig. 5a, which represents the barecloth has an XRD pattern with broad peak at $2\theta \approx 26^\circ$ indicative of turbostratic carbon. As expected, the Cu cloth reveals diffraction peaks of both C and metallic Cu (2θ values of 44° , 50° , 75°) [1, 30] as shown in Fig. 5b.

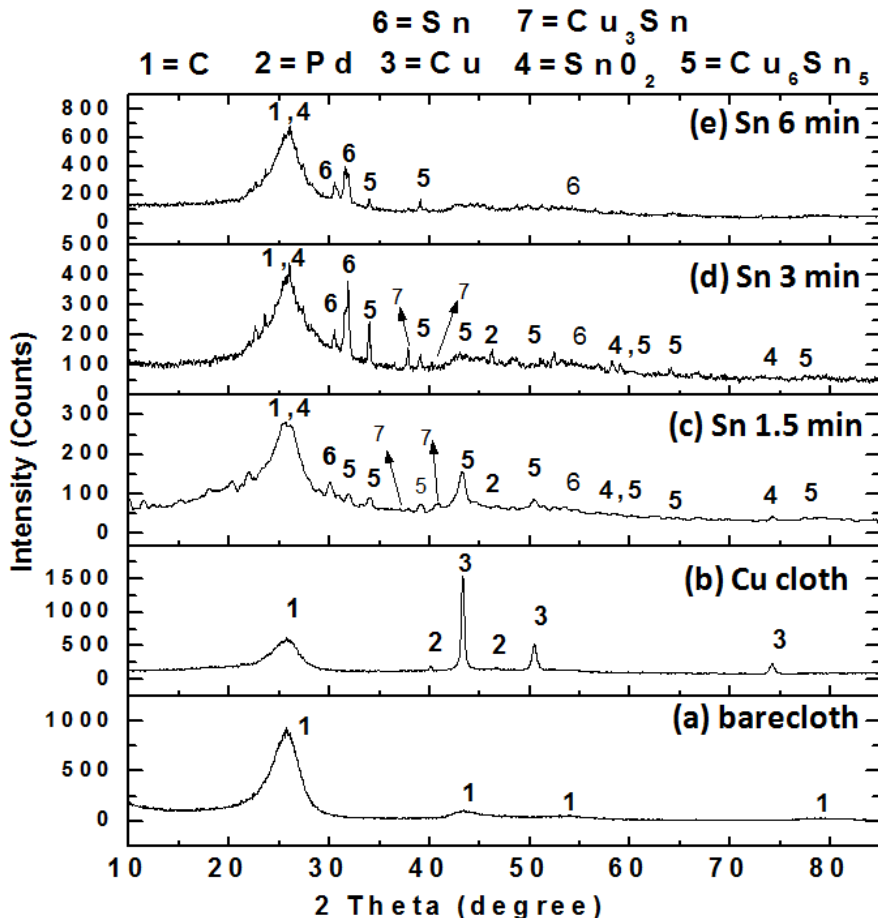


Figure 5. XRD patterns corresponding to (a) barecloth, (b) Cu coated cloth (c) Sn 1.5 min, (d) Sn 3 min, and (e) Sn 6 min.

For the Sn-plated samples shown in Fig. 5c–e, they reveal that metallic Sn was successfully deposited. This confirms prior SEM and EDS observations. Interestingly, the diffraction peaks exhibited by the Sn coated samples are due to Cu_6Sn_5 intermetallic compound at values of $2\theta \approx 32^\circ$, 34.5° , 39° , 44° , 60° , 65° and 78° corresponding to crystal planes (113), (22-3), (204), (71-2), (44-3), and (336), respectively. Similar results were obtained by Park et al [30]. As hypothesized earlier, the Sn 1.5 min sample has preponderance and stronger diffraction peaks due to the Cu_6Sn_5 intermetallics while the diffraction peaks due to Sn are stronger for materials deposited at times longer than 1.5 min. This is in agreement with Park et al.'s suggestion that the Cu_6Sn_5 intermetallic compound formation is at the copper-tin boundary interface [30]. Minor peaks for Cu_3Sn are located at $2\theta \approx 37.5^\circ$ (100) and 41.7°

(002). The peaks for metallic Sn were at $2\theta \approx 31.5^\circ$ (200), 55° (301), and SnO_2 at $2\theta \approx 25^\circ$, 60° and 74° , corresponding to crystal planes (110), (113) and (232), respectively [21]. It is evident that as Sn deposition time increased, the Sn metallic diffraction peaks increased while Cu and Cu_6Sn_5 intermetallic peak decreased which could be ascribed to the higher tin/tin oxide content in the outer layer. This supports the second stage of Sn coating on previously deposited Sn during the electroless coating process. From XRD analysis we believe that our electrode is comprised of crystalline Cu_3Sn_5 - Cu_6Sn_5 -Sn- SnO_2 composite. Furthermore, the size of the crystalline nanoparticles on the surface of the Sn-plated samples were calculated using the Debye Scherrer formula expressed as, $D = 0.9\lambda/\beta\cos\theta$. Here, β is equivalent to the full width at half maximum (FWHM) at an angle θ for a peak, while the wavelength of the X-ray radiation is denoted by λ . The respective particle sizes calculated corresponded very well with SEM, approximately 70 nm, 120 nm and 261 nm, for particles on the Sn 1.5 min, Sn 3 min, and Sn 6 min samples.

The electrode performance depends on its active surface area, hence Brunauer-Emmet-Teller (BET) analysis was used to determine the specific surface areas of the barecloth and the deposited samples. The total specific surface area determined for the barecloth was $104 \text{ m}^2/\text{g}$ while the BET's total specific surface areas evaluated for the coated samples were $169 \text{ m}^2/\text{g}$, $109 \text{ m}^2/\text{g}$, and $6.4 \text{ m}^2/\text{g}$, for the Sn 1.5 min, Sn 3 min and Sn 6 min samples, respectively. At short deposition time, the tin coated sample increased in specific surface area (Sn 1.5 min) while the area decreases with increase in deposition time (for example, Sn 6 min). The reason for this increase is that at short deposition time, 1-D deposited Sn nanoparticles provide large surface area but with increasing deposition time, the deposited coatings of nanoparticles grow into thicker 2D films with decreasing surface areas. Thus, a careful control of deposition thickness or time can be used to synthesize CuSn anodes of varying performances.

3.3 Electrochemical performance

Half-cells assembled with the above electrodes were charged-discharged galvanostatically. The voltages of uncycled half-cells (used as prepared) ranged from 1.9 V for the barecloth to 2.45 V for the Sn 3 min sample. Fig. 6 shows the charge and discharge behavior of the half-cells with barecloth and electroless Cu-Sn anodes obtained at 139 mA/g. The first cycle's discharged capacity profile from as prepared (initial) voltages to 0.007 V for freshly made half-cells is shown in Figs. 6a-d. Furthermore, following the first cycle discharge, all charge and discharge steps completed were carried out between 1.2 V to 0.007 V (vs Li/Li⁺) as shown in Fig. 6a-d. It is important to note that due to the reversible capacity retention for 2nd to 20th cycles, their capacity curves overlap, hence figures 6a - d, their full capacity and voltage profiles are not clearly distinguishable from each other.

It is observed that in Fig. 6a, the first cycle specific discharge capacity for the barecloth was 418 mA/h/g, while the Cu-Sn-plated samples (Fig. 6b-d) first cycle discharge capacities ranged from ~600 mA/h/g for the Sn 6 min to 875 mA/h/g for the Sn 1.5 min. The Sn 3 min sample yielded a first cycle discharge capacity of 620 mA/h/g, a value that lies between the 6 min and 1.5 min samples. The discharge curve representing barecloth begins to plateau close to 0 V which is indicative of Li intercalating C

forming LiC_x. After the first cycle, the barecloth exhibited a first discharge cycle capacity loss of ~ 250 mAh/g. However, the charge/discharge curves after the first and up to the 20th cycle shown in Fig. 6a are seen to overlap each other indicating a reversible capacity retention. Analysis of the 1st discharge curves (lithiation process) for the Sn-coated samples, show a broad plateau/elbow occurring between 1.0 V and 1.2 V in each of the curves.

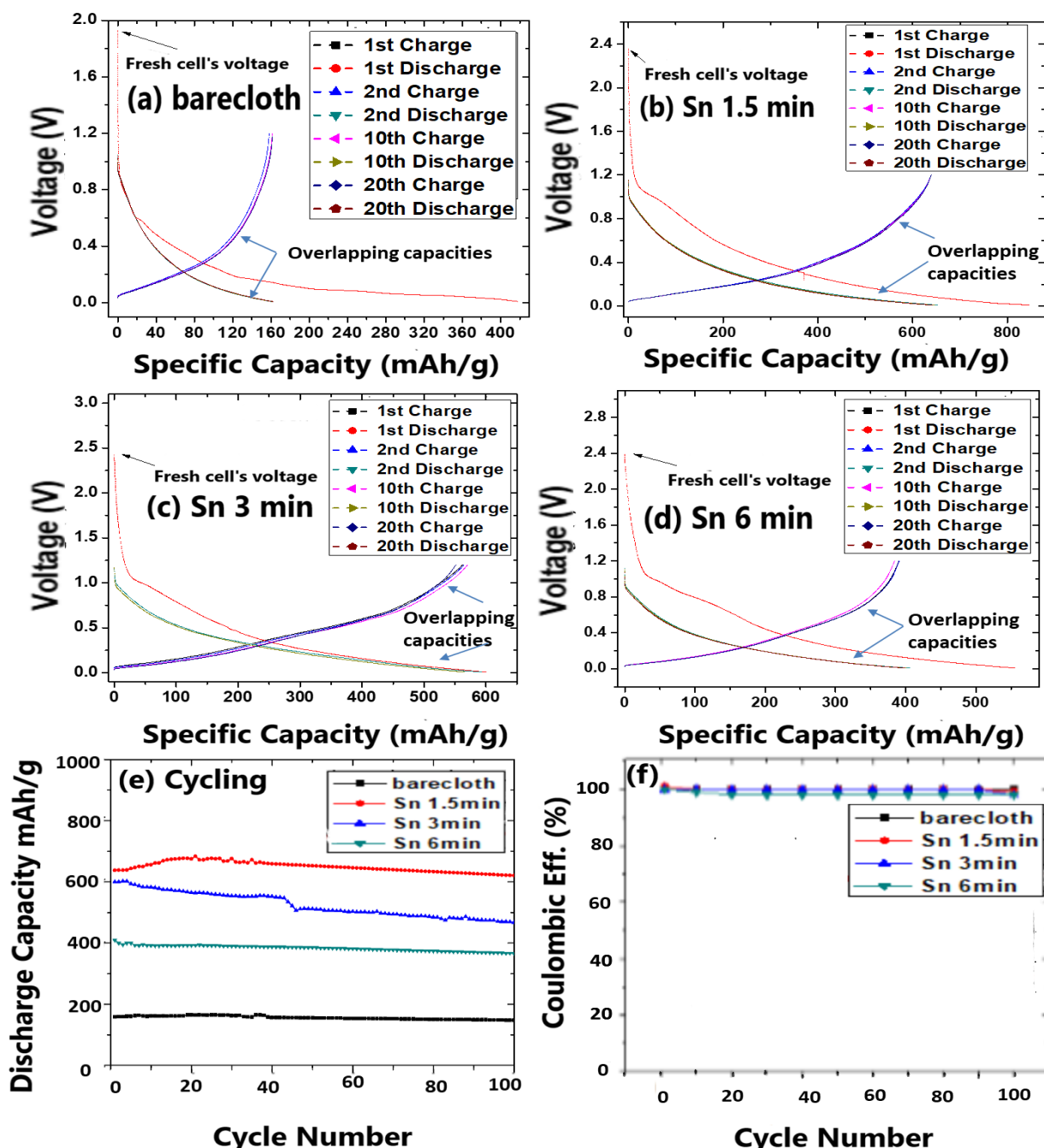
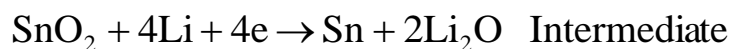


Figure 6. (a-d) Discharge performance at 139 mA/g for freshly made half-cell initially discharged from as prepared potential to 0.007 V and charge/discharge up to 20th cycle, (e) Same half-cells discharged from 2nd cycle to 100th cycle between 1.2 V and 0.007 V, and (f) Coulombic efficiencies for half-cells from 2nd to the 100th cycles.

As the voltage continued to decrease to the lower limit of 0.007 V, a stable decline was noticeable, and this corresponds with CV curves lithiation process. On the strong evidence of the existence and presence of Cu₆Sn₅ in the XRD diffraction peaks seen in all of our Cu-Sn coated samples, we believe our Sn 1.5 min electroless anode is mainly Cu₆Sn₅ intermetallic since it has the most common and highest Cu₆Sn₅ intermetallic peak. Hence, the alloying/dealloying processes of the Cu-Sn coated anodes could follow Eqs. [7] and [8] [1, 15, 16].



Furthermore, XRD indicates the presence of tin oxide and pure tin. Even though, Sn 1.5 min exhibited tin and tin oxide peaks, the Sn 3 min and Sn 6 min anode XRD have higher peak intensities corresponding to higher tin and tin oxide content. The insertion and de-insertion of lithium by these active materials are governed by Eqs. [9] and [10] according to Reddy et al [21] and Watson et al [1].



A high 1st cycle capacity as observed for the Sn 1.5 min was similarly recorded by Kim et al. [31], where they reported a 1st cycle capacity of 2060 mAh/g for ordered mesoporous SnO₂ electrodes. This high first cycle irreversibly discharged capacity is very common for metallic anodes and could be attributed to the decomposition of electrolyte at low voltages thus forming a solid electrolyte interphase (SEI) on the surface of the metal oxide anode [31]. Furthermore, in the same study, Kim et al. found that equation [9] is reversible by use of Synchrotron X-ray diffraction and absorption spectroscopy methods. The reversible decomposition of Li₂O during delithiation allows some of the oxygen to react with Sn forming SnO_x and Li_xO thus leading to capacities much higher than Sn and tin oxide [31]. Their results provided additional evidence to support the high capacity performance of SnO₂ anodes in the present work. As is commonly known, theoretical capacity of SnO₂ is ~783 mAh/g. Hence, our first cycle capacity of 875 mAh/g is within a reasonable range of the above theoretical value for high capacity tin oxide anode performance. Following our 1st cycle discharge, half-cells were charged/discharged continuously at 139 mA/g between 1.2 V and 0.007 V for 100 cycles. Charge/discharge curves for the 2nd, 10th and 20th cycles overlap and are shown in Figs. 6a-d for all cells. In addition, the discharge capacities up to the 100th cycle are shown in Fig. 6e. Similar trends observed for the freshly prepared cells were also seen during the first cycle discharge with the barecloth yielding the lowest capacity value of 158 mAh/g. The trends for the Sn plated samples were the same as observed in Fig. 6b-d with the Sn 1.5 min sample (shortest deposition time) yielding a specific capacity of 638 mAh/g, the Sn 3 min yielded a capacity of 585 mAh/g while the Sn 6 min sample gave a capacity of 408 mAh/g. At the end of the 20th cycle, all the samples had their specific discharge capacities changed. While the specific discharge capacities of the barecloth and Sn 1.5 min increased to 165 mAh/g and 665 mAh/g, respectively, those of Sn 3 min and Sn 6 min samples decreased slightly to 564 mAh/g, and 400 mAh/g, respectively. All the samples, except the Sn 1.5 min sample exhibited a constant discharge curve during the first 20 cycles. A relative rise of 27 mAh/g in discharge capacity between the 1st and 20th cycle exhibited by the Sn 1.5 min sample was similar to the observations made by Shin and coworkers in which capacity increased

with cycle number for Cu₆Sn₅ anode up to the 10th cycle [25]. They attributed this increase to change in morphology and electrolyte accessing new layers of Sn anode due to exposure from the volume change during tin lithium alloying/dealloying process (charging/discharging) [25]. Furthermore, as shown in Fig. 6e, after the 20th cycle, Sn 1.5 min exhibited a stable discharge capacity up to the 30th cycle and a slight capacity decrease up to the 100th cycle. All of the other samples exhibited a stable decrease in discharge capacity profile from the 20th to the 100th cycle. Figure 6f depicts the stable coulombic efficiency for all the samples and all of the efficiency values were greater than 97% which indicates reversibility of all electrodes.

Further insight on the electrochemical behavior of the fabricated Sn anodes was undertaken through cyclic voltammetric (CV) studies at 0.5 mV/s as shown in Fig. 7. Previous study performed by Reddy and coworkers, demonstrated that nano-SnO₂ anode used in lithium battery over the voltage region 0.005 V - 1 V exhibited lower capacity fade than same material tested over 0.005 V - 3.0 V [20]. As such, a best lower and upper limit voltage of 0.007 V and 1.5 V were chosen for our CV studies. The initial three scanning curves obtained from Sn 1.5 min anode is shown in Fig. 7a. For the first cycle's lithiation process, a cathodic peak (C₁) is seen at 0.9 V and as the voltage approaches 0 V, a second cathodic peak (C₂) characteristic of Li alloying with Sn (Li_xSn) emerges (Equation [10]). For the first cycle's delithiation process, a broad anodic peak is located at ~0.7 V. Equation depicting the reversible lithiation/delithiation of the Sn anode material was shown in equation [10].

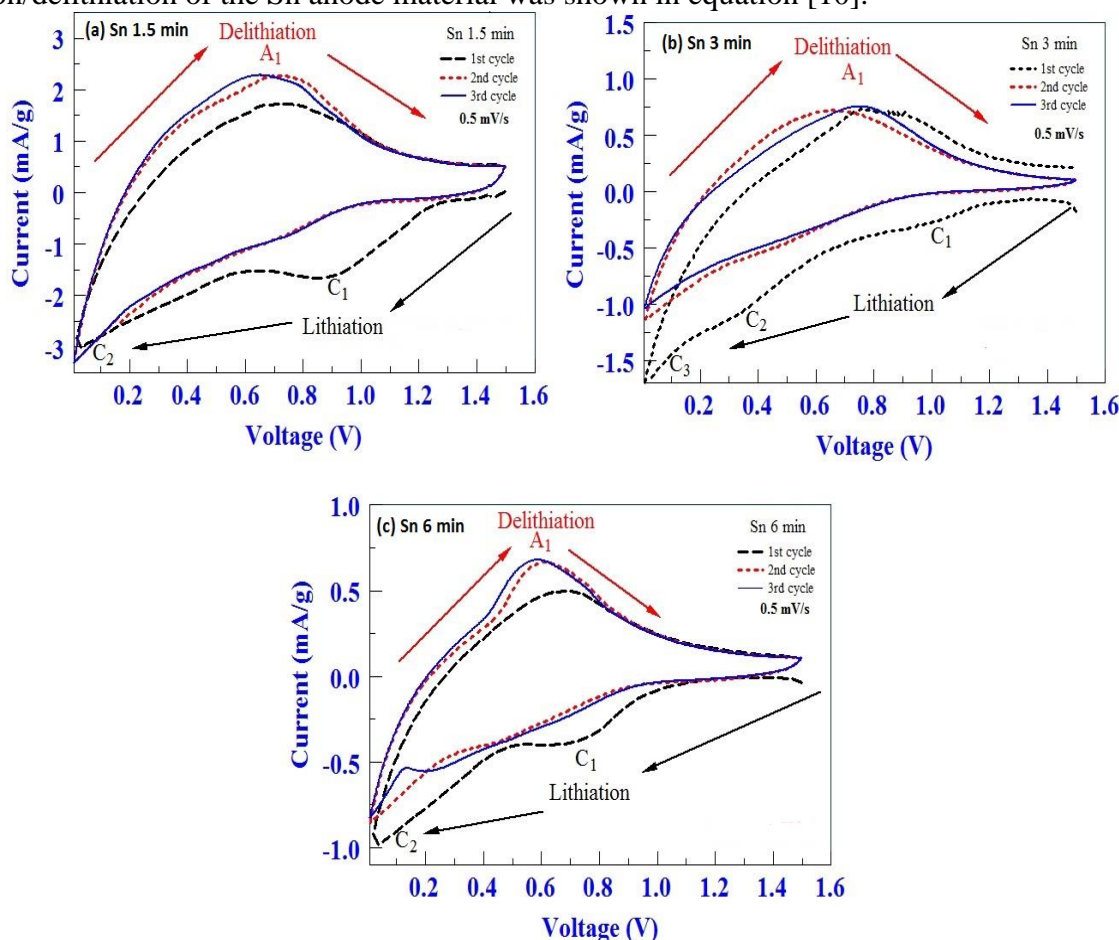


Figure 7. CV results scanned at 0.5 mVs⁻¹ between 0.007 V and 1.5 V for Sn-coated anodes only (a) Sn 1.5 min, (b) Sn 3 min, and (c) Sn 6 min.

During the second and third cycles, a broad lithiation peak was observed at ~0.8 V. This was followed by a peak close to 0.007 V indicative of lithium insertion into Sn, while the peak that was previously present during the 1st lithiation at 0.9 V completely disappeared. The delithiation process for the second and third cycles were characterized by a broad peak (A₁) at ~0.8 V comparable to the first cycle's delithiation process.

The peak current for the first cycle's lithiation reaction is much higher than that of the second and third cycles. We speculate this could be ascribed to an irreversible first cycle capacity loss by the Sn 1.5 min electrode. Fig. 7b presents the first three cyclic voltammograms for the Sn 3 min anode. Unlike the Sn 1.5 min anode, the first cycle's lithiation process for the Sn 1.5 min anode has a broad cathodic peak (C₁) centered at ~1 V which is likely due to decomposition of electrolyte by Sn or SnO₂. A second peak (C₂) 0.4 V and a third (C₃) is seen close to 0.007 V and these are due to lithium alloying with Sn for the formation of Li_ySn [31]. The dealloying of Li_ySn [30], is characterized by an anodic peak (A₁) at ~0.7 V.

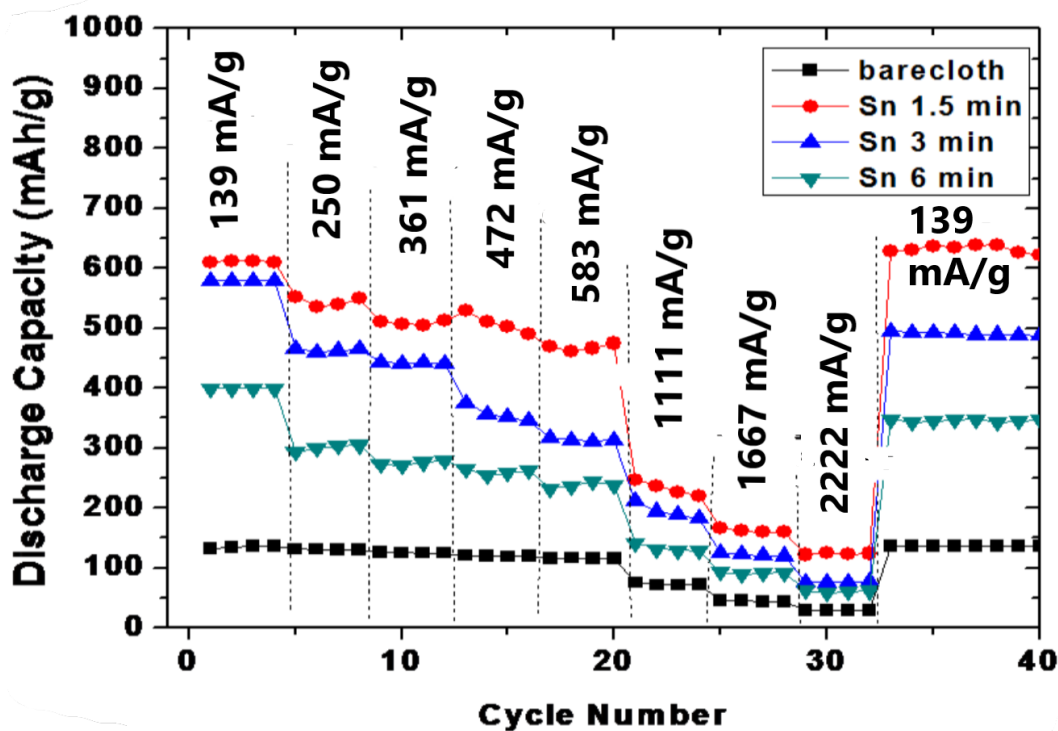


Figure 8. Rate capability studies for half-cells with barecloth and Sn-coated anodes cycled between 0.007 V to 1.2 V.

The second and third scanning cycles', lithiation peaks were very similar at higher voltages, almost overlapping until they approached 0.007 V the peaks were separated. Also, the peak currents close to 0.007 V for these two cycles were much lower than that of the first lithiation process. Analogous to the delithiation process of the first scanning cycle, the second and third cycles exhibited anodic peaks (A₁) centered at 0.7 V and 0.8 V, respectively. Overall, except for minor changes in voltage and peak

currents, the results are similar as in the Sn 1.5 min samples. Similarly, in comparison to the Sn 1.5 min sample, we observe minor shifts in voltages for the Sn 6 min samples as shown in Fig. 7c. For the Sn 6 min anode, a broad cathodic peak (C_1) centered at ~0.75 V and (C_2) at ~0.007 V are observed during the first cycle's lithiation process. Similar results observed for both Sn 1.5 min and Sn 3 min were seen with respect to Sn 6 min sample for both the first and second cycles. The first, second and third delithiation cycles exhibited anodic peaks (A_1) centered between 0.6 V and 0.65 V.

Fig. 8 displays rate-capability studies conducted to determine the performance of the anode materials under different current loads. Similar to the capacity performance shown in Fig. 6, the Sn 1.5 min and Sn 3 min outperformed the barecloth and Sn 6 min half-cells. At 139 mA/g the first cycle specific discharge capacities were ~150 mAh/g, 620 mAh/g, ~590 mAh/g, and ~403 mAh/g for half-cells made from barecloth, Sn 1.5 min, Sn 3 min, and Sn 6 min, respectively. After 32 cycles and at a higher current load of 2222 mA/g, the specific discharge capacities were all lowered with the barecloth yielding the least capacity of 140 mAh/g. As was the case when the current load was lower, the Sn 1.5 min sample with a capacity of 150 mAh/g at the 2222 mA/g load outperformed both the Sn 3 min sample (123 mAh/g capacity) and Sn 6 min sample (101 mAh/g capacity). To determine if the half-cells can retain previous capacity after having been exposed to high currents, cells were tested at 139 mA/g mA from 33rd to 40th cycles (Fig. 8). All cells retained initial capacities with Sn 1.5 min exhibiting highest capacity retention. This implies that our Sn anodes are capable of high rate performance and cyclability without significant capacity loss. It also shows that the thinner film electrodes are more favorable for higher capacity applications.

Following the 40th cycle, we conducted electrochemical impedance spectroscopy (EIS) analysis on charged (~1.20 V) cells made from anodes with and without CuSn and their Nyquist plots are shown in Figs. 9a and 9b. In addition, an equivalent circuit model (ECM) fitting the Nyquist plots is also shown.

In the high frequency area, all Nyquist plots crossed the real axis. Furthermore, there are depressed semicircles in the medium frequency area and a tail extending to the low frequency area of the Nyquist plot. Generally, intercept of the real x-axis in the high frequency is attributed to resistance from the electrolyte and electrode surface (R_s) [32-34]. The resistance due to the transfer of charge (R_{ct}) at the electrode and electrolyte is represented by semicircle in the medium frequency region [32-34]. Finally, the tail extending to the low frequency area commonly called Warburg impedance (W) is associated with the diffusion of lithium ions within the electrode [32-34]. The respective experimental R_s values for the barecloth, Sn 1.5 min, Sn 3 min, and Sn 6 min are 8.5 Ohm, 6.9 Ohm, 6.9 Ohm, and 8.3 Ohm. All cells' R_s values are in the range from 0-10 Ohm matching reports documented elsewhere [35-37]. The ECM fitted R_s values match closely to the experimental values for the barecloth, Sn 1.5 min, Sn 3 min, and Sn 6 min which are estimated to be 8.2 ± 0.3 Ohm, 6.7 ± 0.4 Ohm, 6.8 ± 0.3 Ohm, and 8.1 ± 0.2 Ohm, respectively.

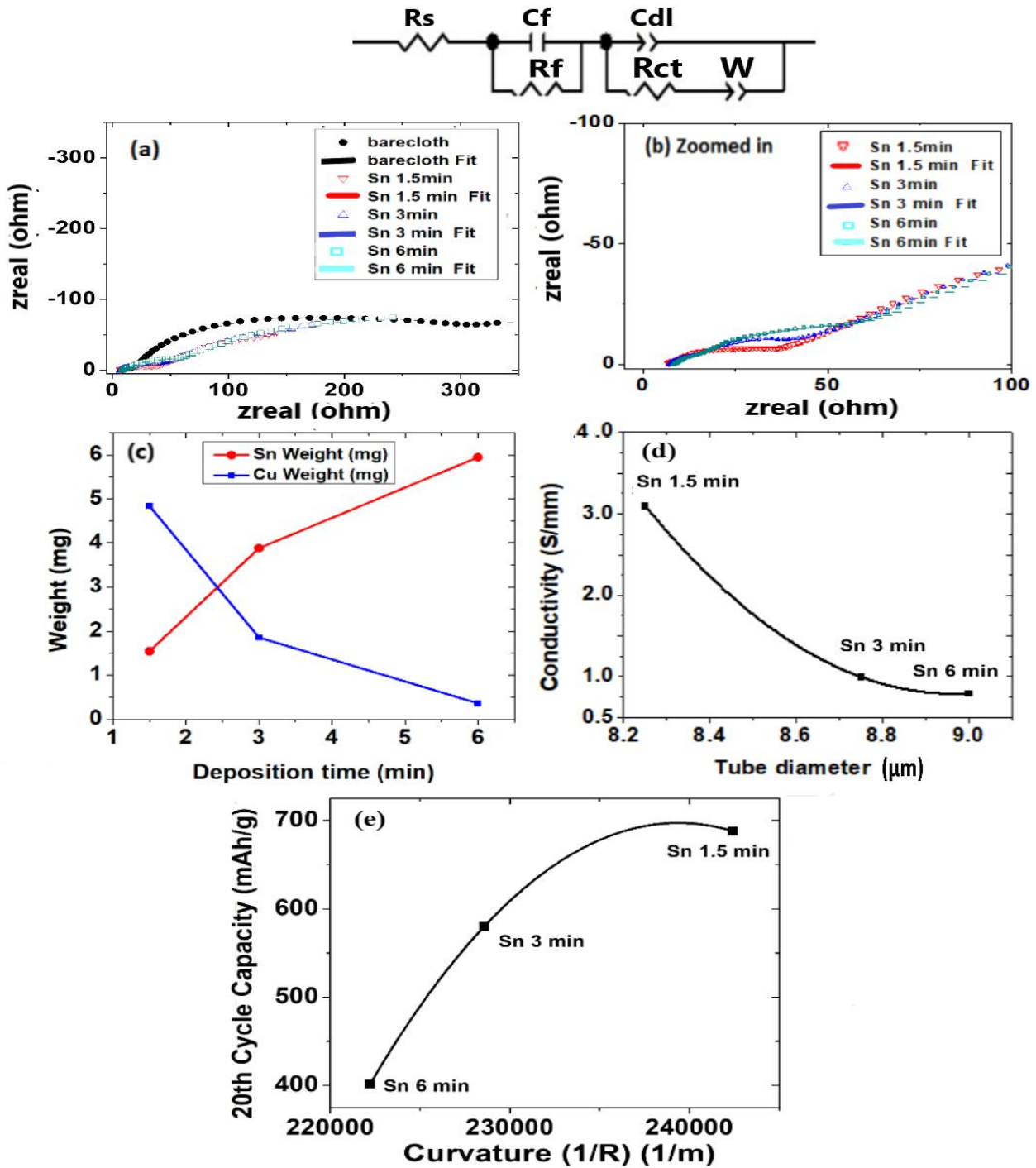


Figure 9. Half-cell equivalent circuit model (ECM) and EIS analysis for (a) barecloth and Sn-coated anodes (b) Sn-coated anodes (zoomed in), (c) Cu and Sn weight variation with deposition times, (d) conductively vs tube radius and (e) capacity vs curvature ($1/R$).

We are particularly interested in the charge transfer processes in the middle frequency region. As such, it was found that the semicircle and the R_{ct} values in that region decreased significantly after Sn deposition as shown in Fig. 9b. R_{ct} values corresponding to barecloth, Sn 1.5 min, Sn 3 min, and Sn 6 min were determined to be 325 Ohm, 39 Ohm, 45 Ohm, and 60 Ohm, respectively. The respective ECM fitted R_{ct} values for barecloth, Sn 1.5 min, Sn 3 min, and Sn 6 min were 324 ± 5 Ohm, 38 ± 2 Ohm, 46

± 3 Ohm, and 60 ± 3 Ohm. Noted is how increase in Sn deposit thickness the R_{ct} values. The low R_{ct} values for the Sn-coated electrodes corroborate with previous cycling results. In addition to the ECM's fitted R_s and R_{ct} , the fitted capacitances attributed to the double layer (C_{dl}) were found to be 102 ± 4 mF/g, 3 ± 0.4 mF/g, 4 ± 0.3 mF/g, and 5.8 ± 0.4 mF/g, respectively.

3.4. Reasons for the spectacular performance of short time-deposited CuSn electrode

It is evident that anodes with shorter Sn deposition time or lower Sn wt. %, results in better electrochemical performances as indicated by the cycling tests, rate-capability tests, and EIS analysis. Therefore, lower deposition times might be favorable in an effort to lower unused Sn and maximize the electrochemical performance of the Cu-Sn anode energy storage material. We are of the opinion that the effect of deposition times on electrode's performances could be explained using relationships with Cu to Sn content, particle size, conductivity, diffusion coefficient of Li^+ and activity of tube related to the tube diameter or curvature. These are explained as follows:

(1) As shown in Fig. 9c, Sn's content increased with increasing deposition time while the content of copper decreased. Since Cu has excellent electrical conductivity, it is our belief that the higher Cu content in the Cu-Sn alloy at lower Sn deposition times could improve the electrochemical performance of the Cu-Sn anode through its enhancement of the electrical contact and electronic conductivity of the resulting Cu-Sn alloy. As such, prior to half-cells' assembly, the electrical sheet resistance of the barecloth, Cu cloth, and Sn coated Cu cloths were measured. The resistances were used to calculate electrical sheet conductivity and we found that the barecloth has a sheet conductivity of 0.31 S/mm. With electroless deposition of copper for 1 hour, the sheet conductivity increased dramatically (as expected) to 6.7 S/mm. However, with the deposition of Sn on the copper, the conductivity decreased with increased deposition time. For the Sn 1.5 min, Sn 3 min, and Sn 6 min samples, their respective conductivities values were 3.1 S/mm, 1 S/mm, and 0.8 S/mm as plotted in Fig. 9d. Furthermore, Liu et al. reported that during lithiation and delithiation processes, higher copper content helps to buffer and stabilize Sn particle expansion resulting in extended cycling and capacity retention [13].

(2) We also believe that only thin layers of deposited Sn participate in the redox reactions i.e. alloying dealloying. If this is correct, lower deposition time would have smaller particles or thinner layers of tin with higher surface areas for redox reactions to occur. That is, at short deposition times, Sn nanoparticles equivalent to 1D particles are active with large surface area. This is supported by the present work where the respective BET surface areas for Sn 1.5 min, Sn 3 min, and Sn 6 min were 169 m²/g, 109 m²/g and 6.4 m²/g. As seen in our SEM image, Sn 1.5 min had thinnest layer of Sn deposited/coated and smallest Sn grains (75 nm) followed by Sn 3 min (128 nm) and Sn 6 min (270 nm). Also, the XRD results show, the Sn 1.5 min sample has large composition of CuSn intermetallic. Particle size estimates were 70 nm for Sn 1.5 min, 120 nm for Sn 3 min and 261 nm for the Sn 6 min sample. The intermetallics and smaller Sn particles or thinnest layers can accommodate large stress imparted during alloying-dealloying process thus, reducing Sn pulverization. Longer deposition times increases thicker layers of Sn on top of the CuSn intermetallic with limited surface areas. Unlike the thin deposit, the thick Sn layer does not accommodate electrolyte penetration as well as stress thus resulting in

pulverization and poor capacity retention. This was also observed by Ulus and coworkers. They reported that thick Sn metal anodes are more at risk of stress damage during cycling than thinner Sn metal anodes [38]. In addition, Deng and coworkers reported that anodes made from 15 minute tin deposition material performed worse than 10 minute anode material fabricated by direct current sputtering [33]. It appears that this observation maybe common to several investigators and hence, longer Sn deposition times may not be most favorable for anodes with capacity retention and long-term cycling. In our analysis, we have found that the thicker electrodes with lower surface areas limit the transport of lithium ions. Using the cyclic voltammetry peak currents and other parameters described by the Randles-Sevcik equation, we estimated the diffusion coefficient for Li^+ chemical specie using equation 11:

$$I_p = 0.4463F \left(\frac{F}{RT} \right)^{\frac{1}{2}} AD_{\text{Li}^+}^{\frac{1}{2}} C v^{1/2} \quad \text{or} \quad D_{\text{Li}^+} = \left(\frac{I_p}{0.4463F \left(\frac{F}{RT} \right) AC v^{1/2}} \right)^2 \quad [11]$$

Where, R=gas constant, T=temperature, F=Faradays constant (C/mol), A=area of electrode (cm^2), C=species concentration (mol/cm^3), D_{Li^+} =diffusion coefficient (cm^2/s), and v=scan rate (V/s).

Using the peak current from CV curves' shown in Fig. 7 and other results from equation 11, lithium ions' chemical diffusion coefficient was calculated for the electrodes in the three Sn-Cu coated half-cells. For the Sn 1.5 min, Sn 3 min, and Sn 6 min electrodes, results showed that the average chemical diffusion coefficients (D_{Li^+}) were $6.6 \times 10^{-13} \text{ cm}^2/\text{s}$, $3.7 \times 10^{-13} \text{ cm}^2/\text{s}$, and $1.1 \times 10^{-13} \text{ cm}^2/\text{s}$, respectively. As seen, the mobility of the lithium ion is fastest in the higher surface area with smaller particle sizes and lower time deposited electrodes. The route of lithium ions in the bulk electrodes is vital to ensure suitable quantity of specie (Li^+) to carry on the redox reaction occurring. Therefore, the electrode with the highest D_{Li^+} (mobility), is expected to display better performance electrochemically especially at high current loads/densities. This could be an additional factor leading to the highest peak current and capacity exhibited by Sn 1.5 min half-cell.

(3) Lastly, nano and micro dimensions offered by the Sn coated tubes increase the active materials' chemical reactivity in the surrounding electrolyte while enhancing stable cycling despite volume expansion [39]. As reported by Shafiei et al. recently, these characteristics are attributed to the curvature of the Sn coated tubes, where curvature is defined as $1/R$ (R = radius of Sn coated tube) [41]. Using the stable 20th cycle results, the relationship between the curvature and capacity shown in Fig. 9e can be fitted and represented by a simple polynomial (Eqs. [12]) over the various deposition times as:

$$\begin{aligned} Y &= ax^2 + bx + c \\ &= -1.002 \times 10^{-6}x^2 + 4.797 \times 10^{-1}x - 5.671 \\ &\quad \times 10^4 \end{aligned} \quad [12]$$

Where Y = specific capacity (dependent variable) in mAhg^{-1} , x is the curvature (independent variable) of tube ($1/R$) in m^{-1} , a (cross-sectional areal capacity in $\text{mAhg}^{-1}\text{m}^2$) and b (radial length capacity in mAhg^{-1}m) are coefficients while c is a constant in mAhg^{-1} . It is to be noted that this is not a relationship that can be generalized and used for all systems. It is only specific for the conditions of the present work.

Observation of the fitting and Eq. [12] indicates that for higher capacity to be obtained, we should engineer smaller diameter SnCu tubes. The fitting therefore indicates that tubular SnCu anode surfaces

with high curvature (small radius) and high surface area allow deep penetration of electrolyte and are more favorable for reversible and high capacity performances instead of planar SnCu anode surfaces. For instance, for a planar anode, R approaches infinity, while x approaches zero and thus the value of Y, specific capacity approaches its minimum value. Therefore, it corroborates why some researchers observe extremely high capacity when lower dimension tubes such as carbon nanotubes are used as template for Sn growth.

In our observations, lower deposition time resulted in smaller diameter Sn tubes. Therefore, amongst the three samples studied, Sn 1.5 min anode with lowest R and highest curvature exhibits highest capacity retention and provided most stable long-term cycling (20 to 100 cycles) followed by Sn 3 min and Sn 6 min. Curvature of the SnCu tubes ($1/R$) is instrumental to capacity retention of the anode materials. Higher curvature is attributed to smaller tube radius, and this is beneficial for increase tube's surface area available for redox reaction or charge transfer to occur between electrolyte and active particle's/anode's surface. High surface area tube with nanoparticles accommodates more volume expansion while reducing pulverization and maintaining electrical contact between electrochemically active surfaces for lithiation or delithiation thus leading to repeated capacity retention after each cycle. Fig. 9e suggests that a deposition time slightly shorter than that used for Sn 1.5 min sample will provide a better performing anode with a capacity of ~700 mAh/g and curvature of $\sim 237000\text{ m}^{-1}$. This can be verified as part of the optimization of described method. An increase in electronic conductivity, surface area, and curvature of the fibrous SnCu coated tubes, along with the porous mesh-like electrodes framework lead to higher mobility of Li^+ ions and thus current (reactivity) leading to increase in capacity. From our observations, the mobility, conductivity, curvature and capacity of the electrodes are influenced by the characteristic of the anodes which are attributed to Sn coating times or deposited particle sizes.

4. CONCLUSIONS

In this study, we demonstrated a technique and conditions necessary to fabricate flexible, standalone and binder-free Cu-Sn anode (comprising of Cu_3Sn , Cu_6Sn_5 , Sn, SnO_2) using electroless coating/deposition of Sn on copper coated carbon cloth substrate. The key process parameter for high performance CuSn anode is the deposition time required to maintain a 1-D deposit of Sn nanoparticles with large surface area, high conductivity and able to accommodate stress with minimal pulverization. Electroless coating approach reduced costly extended drying steps used in the conventional fabrication methods since the use of a binder and mixing of a slurry are eliminated from this electrode's synthesis. After 100 cycles, Sn anodes deposited for 1.5 and 3 minutes exhibited high capacity and repeated cyclability of ~608 mAh/g and ~495 mAh/g, respectively when tested at 139 mA g^{-1} . Moreover, both anodes display low capacity degradation at high current loads. Cyclic voltammetry results showed that the redox reactions on the surface of Sn 1.5 min and Sn 3 min anodes are efficient and reversible (highest peak current). Impedance results indicated that half-cells made from Sn 1.5 min and Sn 3 min anodes exhibited reasonably low cell resistance. The XRD results demonstrate that the short time deposits have majorly CuSn intermetallics components with minimal Sn/ SnO_2 coverage. Overall, this electroless

coating/deposition approach has proven to be a facile viable binder-free alternative to other common methods used for Sn anode fabrication.

ACKNOWLEDGEMENTS

Funding for this project was provided by ERC Program of the National Science Foundation Cooperative Agreement Number EEC-08212121. We wish to acknowledge Dr. Eric Lochner (FSU Physics) and Bob Goddard (National High Magnetic Field Laboratory, Tallahassee Florida) for their help with the characterizations.

References

1. V. Watson, Y. Yeboah, M. Weatherspoon, J. Zheng, and E. E. Kalu, *Int. J. Electrochem. Sci.*, 13 (2018) 7968.
2. C. Fu, C. Song, L. Liu, W. Zhao, and X. Xie, *Int. J. Electrochem. Sci.*, 11 (2016) 154.
3. F. Zhang, D-D. Qi, and X.-G. Zhang, *Int. J. Electrochem. Sci.*, 11 (2016) 189.
4. J. Qu, Y. Yang, Z. Chen, Y. Ren, J. Ding, and N. Yuan, *Int. J. Electrochem. Sci.*, 11 (2016) 4389.
5. J.-H. Lee, J.S. Kim, Y.C. Kim, D.S. Zang, and U. Paik, *Ultramicroscopy*, 108 (2008) 1256.
6. C.-C. Li, Y.H. Wang, and T.Y. Yang, *J. Electrochem. Soc.*, 158 (2011) A828.
7. C.-C. Li, X.W. Peng, J.T. Lee, and F.M. Wang, *J. Electrochem. Soc.*, 157 (2010) A517.
8. M. Sun, H. Zhong, S. Jiao, H. Shao, and L. Zhang, *Electrochimica Acta*, 127 (2014) 239.
9. A.R. Kamali, and D.J. Fray, *Rev. Adv. Mater. Sci.*, 27 (2011) 14.
10. X. Chen, J. Guo, K. Gerasopoulos, A. Langrock, A. Brown, R. Ghodssi, J.N. Culver, and C. Wang, *J. Power Sources*, 211 (2012) 129.
11. A.N. Dey, *J. Electrochem. Soc.*, 118 (1971) 1547.
12. M. Winter, and J.O. Besenhard, *Electrochim. Acta*, 45 (1999) 31.
13. S. Liu, Q. Li, Y. Chen, and F. Zhang, *J. Alloys and Compounds*, 478 (2009) 694.
14. I. Igorevna, and T. Bushkevich, *J. Alloys and Compounds*, 415 (2006) 229.
15. K.C. Hewitt, L.Y. Beaulieu, and J.R. Dahn, *J. Electrochem. Soc.*, 148 (2001) A402.
16. N. Tamura, R. Ohshita, M. Fujimoto, M. Kamino, and S. Fujitani, *J. Electrochem. Soc.*, 150 (2003) A679.
17. F. Ozela, M. Kusa, A. Yar, E. Arkan, M. Z. Yigit, A. Aljabour, S. Büyükceli, C. Tozlu, and M. Ersoz, *Materials Letters*, 140 (2015) 23.
18. P. Nithyadharseni, M.V. Reddy, M. Kalpanad, and B.V.R. Chowdari, *Electrochimica Acta*, 161 (2015) 261.
19. P. Nithyadharseni, M.V. Reddy, B. Nalini, T.R. Ravindran, B.C. Pillai, M. Kalpana, and B.V.R. Chowdari, *Materials Research Bulletin*, 70 (2015) 478.
20. M.V. Reddy, L.Y. Tse, W.K.Z. Bruce, and B.V.R. Chowdaria, *Materials Letter*, 138 (2015) 231.
21. M.V. Reddy, L.Y.T. Andreea, A.Y. Ling, J.N.C. Hwee, C.A. Lin, S. Admas, K.P. Loh, M.K. Math, K.I. Ozoemen, and B.V.R. Chowdari, *Electrochimica Acta*, 106 (2013) 143.
22. Y. Yu, L. Gu, C. Wang, A. Dhanabalan, P.A. van Aken, and J. Maier *J. Angew. Chem. Int. Ed.*, 48 (2009) 6485.
23. X. W. Lou, D. Deng, J.Y. Lee, and L.A. Archer, *Chem. Materials*, 20 (2008) 6562.
24. W.J. Lee, M.-H. Park, Y. Wang, J.Y. Lee, and J. Cho, *Chem. Comm.*, 46 (2010) 622.
25. H.-C. Shin, and M. Liu, *Advance funct. Mater.*, 15 (2005) 582.
26. L. Xue, Z. Fu, Y. Yao, T. Huang, and A. Yu, *Electrochemical Acta*, 55 (2011) 7310.
27. G. Cui, N. Li, and J. Zhao, *J. Electrochem. Soc.*, 153(12) (2006) C848.
28. E. Huttunen-Saarivirta, and T. Tiainen, *J. Mater. Process. Technol.*, 170(1-2) (2005) 211.
29. H.T. Ng, S.F.Y. Li, L. Chan, F.C. Loh, and K.L. Tan, *J. Electrochem. Soc.*, 145(9) (1998) 3301.

30. H. Park, J.H. Um, H. Choi, W-S. Yoon, Y.-E. Sung, and H. Choe, *Applied Surface Science*, 399 (2017) 132.
31. H. Kim, G.O. Park, Y. Kim, S. Muhammad, J. Yoo, M. Balasubramanian, Y.-H. Cho, M-G. Kim, B. Lee, K. Kang, H. Kim, J. M. Kim, and W.-S. Yoon, *Chem. Mater.*, 26 (2014) 6361.
32. S. Han, B. Jang, T. Kim, S.M. Oh, and T. Hyeon, *Adv. Funct. Mater.*, 15 (2005) 1845.
33. P.L. Moss, G. Au, E.J. Plitcha, and J.P. Zheng, *J. Electrochem. Soc.*, 155 (2008) A986.
34. J. Gomez, R. Nelson, E.E. Kalu, M.H. Weatherspoon, and J.P. Zheng, *J. Power Sources*, 196 (2011) 4826.
35. D.Y.W. Yu, C. Fietzek, W. Weydanz, K. Donoue, T. Inoue, H. Kurokawa, and S. Fujitania, *J. Electrochemical Society*, 154 (2007) A253.
36. M. Gaberscek, J. Moskon, B. Erjavec, R. Dominko, and J. Jamnik, *Electrochemical and Solid-State Letters*, 11 (2008) A170.
37. X. Fan, X. Tang, D. Ma, P. Bi, A. Jiang, J. Zhu, and X. Xu, *J. Solid State Electrochem.*, 18 (2014) 1137.
38. L. Zhong, C. Beaudette, J. Guo1, K. Bozhilov, and L. Mangolini, *Sci. Rep.*, 6 (2016) 1.
39. A. Ulus, Y. Rosenberg, L. Burstein, and E. Peled, *J. Electrochemical Society*, 149(5) (2002) A634.
40. Q. Deng, Z. Huang, X. Dai, Y. Wang, Z. Li, and J. Li, *J. Solid State Electrochemistry*, 19 (2015) 1765.
41. M. Shafiei, and A.T. Alpas, *J. Power Sources*, 196 (2011) 7771.

© 2019 The Authors. Published by ESG (www.electrochemsci.org). This article is an open access article distributed under the terms and conditions of the Creative Commons Attribution license (<http://creativecommons.org/licenses/by/4.0/>).